PROCEEDINGS OF SCIENCE

Investigation of the η'-η_c-mixing with improved stochastic estimators

Christian Ehmann* **and Gunnar S. Bali**
Institut für Theoretische Physik, Universität Regensburg,
93040 Regensburg, Germany
E-mail: christian.ehmann@physik.uni-regensburg.de,
gunnar.bali@physik.uni-regensburg.de

Charmonia are flavour singlet mesons and thus in principle contributions from disconnected quark line diagrams might affect their masses, either directly or via mixing with other flavour singlet channels. We present a first study that takes both effects into account. We employ improved stochastic all-to-all propagator techniques (including new methods) to calculate the diagrams that appear within the mixing matrix between the η' and the η_c. The runs are initially performed on $N_f = 2$ $16^3 \times 32$ configurations with the non-perturbatively improved Sheikholeslami-Wilson action, both for valence and sea quarks.

The XXVI International Symposium on Lattice Field Theory
July 14-19 2008
Williamsburg, Virginia, USA

*Speaker.

1. Introduction

Lattice calculations of the charmonium S-wave hyperfine splitting tend to underestimate the experimental value of 117 MeV [1 – 6]. However, in none of these studies all systematics have been addressed as yet. One such source of error is the difference of the running of the QCD coupling between low momenta $\simeq mv^2$ that determine the spin averaged splittings and the high momenta $> mv$ responsible for the fine structure. Too few or too heavy sea quark flavours will result in a comparably smaller coupling at high momenta, resulting in such an underestimation [7]. Furthermore, the finestructure is particularly sensitive to short distance physics, necessitating a careful extrapolation to the continuum limit.

Here we will investigate the effect of quark-antiquark annihilation diagrams, the neglection of which might be an additional source of the discrepancy. Although heavy, compared to the chiral symmetry breaking scale, the η_c state might still sense some remnant axial $U(1)$ effect that could result in an upward mass shift, perhaps of a few MeV. Another aspect is the mixing with other flavour singlet states, e.g. the pseudoscalar glueball or the η' meson and its radial excitations.

We study both effects: quark annihilation diagrams [1 – 3] and mixing with the η', hence called η since we have $N_f = 2$. To investigate this mixing we construct a correlation matrix containing both light and charm quark operators, the calculation of which requires all-to-all-propagators. The eigenvalues and appropriately normalized eigenvectors of this matrix are indicative of the magnitude of mixing between the two sectors.

2. Simulation details

Our runs are performed on $N_f = 2$ $16^3 \times 32$ configurations generated by the QCDSF collaboration [8], with a lattice spacing $a \approx 0.1145\,\mathrm{fm}$, obtained from the chirally extrapolated nucleon mass. For valence and sea quarks we use the clover action, with c_{sw} determined non-perturbatively. The charm quark mass was set by tuning the spin-averaged charmonium mass $\frac{1}{4}(m_{\eta_c} + 3m_{J/\Psi})$ to its experimental value. The pion on these lattices is rather heavy: $m_\pi = 1007(2)\,\mathrm{MeV}$. However, this reduces the mass gap between the η and the η_c which might enhance mixing effects. Computations took place on the local QCDOC using the Chroma software library [9]. We utilized 100 effectively de-correlated configurations, where on each 200 independent stochastic estimates were created.

3. All-to-all propagator techniques

In order to calculate the quark-antiquark annihilation diagrams, we require propagators from any start to any end point. An exact inversion of the Dirac Operator M is not feasible in terms of the memory requirements and computation time. Hence we calculate unbiased stochastic estimates of these all-to-all propagators. We define random noise vectors $|\eta^i\rangle$, $i = 1, \ldots, N$ with components,

$$\eta^i_{\alpha,a,x} \quad = \quad \frac{1}{\sqrt{2}}(v + iw)\,, \qquad v, w \in \{\pm 1\}\,. \tag{3.1}$$

We solve the linear problem for these N sources:

$$|s^i\rangle = M^{-1}|\eta^i\rangle\,, \tag{3.2}$$

where,

$$\frac{1}{N}\sum_i \eta^i_{\alpha,a,x}\eta^{i*}_{\beta,b,y} = \delta_{x,y}\delta_{a,b}\delta_{\alpha,\beta} + O\left(\frac{1}{\sqrt{N}}\right). \tag{3.3}$$

The propagator M^{-1} can now be estimated as follows:

$$\overline{|s\rangle\langle\eta|} := \frac{1}{N}\sum_i |s^i\rangle\langle\eta^i| = \frac{1}{N}\sum_i M^{-1}|\eta^i\rangle\langle\eta^i| \quad = \quad M^{-1}\left[\mathbb{1} + O\left(1/\sqrt{N}\right)\right]. \tag{3.4}$$

We obtain the full propagator plus off-diagonal noise term, which vanish like $\frac{1}{\sqrt{N}}$. We apply several improvement schemes to reduce this stochastic noise.

3.1 Staggered spin dilution (SSD)

Usually a propagator receives its dominant noise contributions from the stochastic sources that are closest to the sink, in terms of Euclidean distance or in spinor space. Such contributions can be reduced in a straight forward way by *partitioning* (or "diluting") spacetime, colour and/or spin into n_p disjoint subspaces [10, 11]. The subsequent reconstruction of an all-to-all propagator from partition-to-all propagators comes at a significant computational overhead (proportional to n_p). Sometimes the resulting statistical error however is reduced by more than a factor $\propto n_p^{-1/2}$, justifying this method.

Spin partitioning is usually achieved by employing four sets of noise vectors, each with only one spin component different from zero. Obviously, this is not the only possible pattern. We find that especially for heavy quarks other distributions of the spin components are superior to this standard scheme. We attempt to exploit the fact that for large quark masses the Wilson-Dirac operator only weakly couples the upper and the lower spinor components and we devise a partitioning pattern where at different spacetime positions different spin components are stochastically seeded: an upper component site should only neighbour lower component sites and vice-versa. We found a scheme to be particularly effective, which we coin *Staggered spin dilution (SSD)*. This is defined and compared to the standard dilution scheme in the left column of Fig. 1. The numbers indicate the spinor component which is different from zero. The right column of Fig. 1 shows the corresponding nearest neighbour coupling strength, where red means "strong" and green means "weak".

3.2 Hopping parameter acceleration (HPA)

This technique [12 – 14] is based on the *Hopping Parameter Expansion (HPE)* of a Wilson-type Dirac operator $M = \mathbb{1} - \kappa D$, where D only couples nearest neighbours:

$$M^{-1} = (\mathbb{1} - \kappa D)^{-1} = \mathbb{1} + \kappa D + \ldots + (\kappa D)^{n-1} + (\kappa D)^n \sum_{i=0}^{\infty} (\kappa D)^i \tag{3.5}$$

$$\Rightarrow (\kappa D)^n M^{-1} = M^{-1} - (1 + \kappa D + \ldots + \kappa D^{n-1}) : \tag{3.6}$$

the multipication of the propagator by $(\kappa D)^n$ subtracts all the terms up to $n-1$ hops, cancelling the corresponding fluctuations from noisy source positions near the sink. While this reduces the variance, the signals of Green functions for distances larger than $n-1$ hops remain unaffected. Applications are the calculation of correlation functions with time separations $t \geq na$ or of disconnected loops where the first $n-1$ terms are either calculated exactly or vanish identically. The

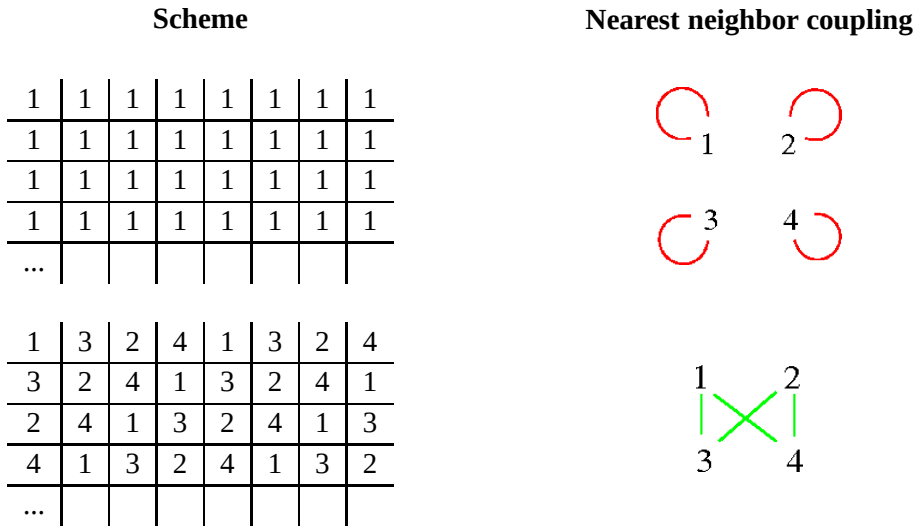

Figure 1: The left column shows the dilution schemes in two dimensions. The corresponding coupling is sketched in the right column (green is weak, red is strong coupling).

effect of HPA on the pseudoscalar loop calculated using the Wilson action at the charm mass is plotted on the left hand side of Fig. 2. (The first multiplication has no effect since $\mathrm{Tr}\,\gamma_5$ is zero anyway.) This technique is particularly suitable for heavy quarks where the rate of convergence of HPE improves but significant gains have also been reported for light quarks [15].

3.3 Recursive noise subtraction (RNS)

In addition we use an algebraic improvement scheme (RNS) where the off-diagonal terms appearing in Eq. (3.4) are calculated and subtracted by hand. The idea can be illustrated as follows:

$$M^{-1} = \overline{|s\rangle\langle\eta|} + M^{-1}(1-\overline{|\eta\rangle\langle\eta|}) \approx \overline{|s\rangle\langle\eta|} + \overline{|s\rangle\langle\eta|}(1-\overline{|\eta\rangle\langle\eta|})\,. \tag{3.7}$$

The outer product $\overline{|\eta\rangle\langle\eta|}$ should be truncated to diagonal blocks of a dimension that is small compared to $\sqrt{N}$. We use the 12-dimensional colour $\otimes$ spin subspace and display a scatter plot between estimates on the right hand side of Fig. 2. The correlation angle is close to $\pi/4$: adding the two terms as suggested will result in a reduced stochastic error. In principle one can make a more general ansatz like $\overline{|s\rangle\langle\eta|}[\mathbb{1}+\alpha(\mathbb{1}-\overline{|s\rangle\langle\eta|})+\beta(\mathbb{1}-\overline{|s\rangle\langle\eta|})^2+\cdots]$ and optimize the parameters $\alpha,\beta,\ldots$ accompanying the different estimates of *zero* to minimize the noise in a given channel. Here we use $\alpha=1,\beta=0$.

3.4 Truncated solver method (TSM)

For the computation of the light quark loops appearing in the mixing matrix we apply the TSM using the BiCGStab solver. For details see [15].

3.5 Reduction of the total computational effort

We summarize the effect of the tested improvement schemes on the disconnected part of the zero-momentum projected η_c two-point function $\langle\,\mathrm{Tr}(M^{-1}\gamma_5)\,\mathrm{Tr}(M^{-1}\gamma_5)\,\rangle$ at $t=0$ in Table 1. The

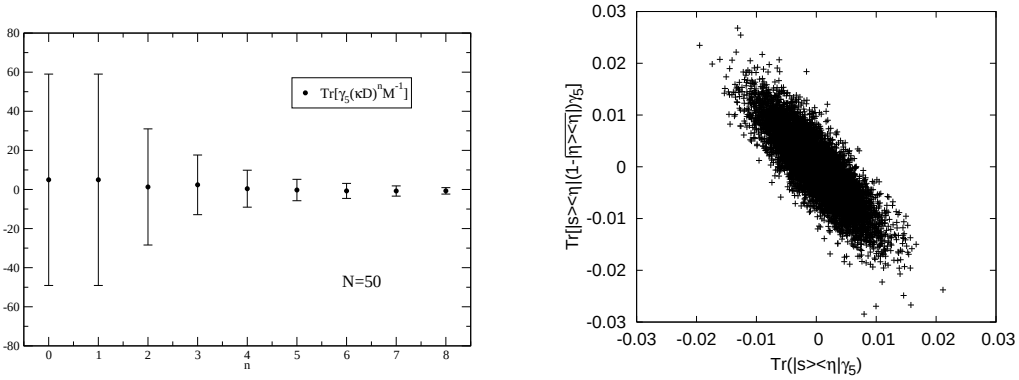

Figure 2: The effect of the HPA on the error of the pseudoscalar correlator for the Wilson action at the charm mass is shown on the left. On the right the RNS scatter plot is displayed.

gain is in terms of real computer time. n is the power of κD applied to the sink vector. Our use of the clover action to calculate $\mathrm{Tr}(M^{-1}\gamma_5)$ restricts us to $n < 3$, since $\mathrm{Tr}(D^2\gamma_5) \propto F\tilde{F} \neq 0$. In principle one could calculate these terms by hand and add them back in again. With colour and staggered spin dilution and two applications of κD we obtain a net gain factor of almost 12. Note that these numbers do not include the effect of the TSM that we only use for the light quark propagators. Also we have not yet combined RNS with the partitioning methods.

n	no	spin	color	color + spin	SSD	SSD + color	RNS
0	1	1.43	1.80	2.52	1.97	3.63	1.87
2	2.89	6.32	5.06	10.24	7.16	11.80	5.44

Table 1: Effective gain of the different improvement schemes. n is the power of κD used in HPA.

4. The mixing

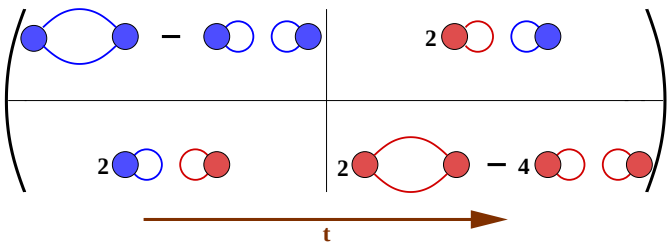

Figure 3: The mixing matrix. The blue lines indicate charm quark, the red ones light quark propagators.

Now that we are equipped with techniques to address quark-antiquark-annihilation diagrams reliably, we calculate the elements of the mixing matrix. Both charmonium and light meson interpolators are included, three in each sector: $(c\bar{c})_0$, $(c\bar{c})_{10}$, $(c\bar{c})_{80}$, $(u\bar{u})_0$, $(u\bar{u})_5$, $(u\bar{u})_{40}$, where the subscript indicates the number of Wuppertal smearing steps with $\delta = 0.3$, employing spatial APE smeared ($n_{APE} = 15$, $\alpha = 0.3$) parallel transporters. These smearing parameters were determined

by optimizing the effective masses within the two sectors, ignoring disconnected contributions, see [5]. In Fig. 3 we sketch the two by two mixing matrix, where the blue lines represent charm and the red lines light quark propagation. The prefactors are due to the two mass degenerate light flavours.

The variational method is applied to the mixing matrix by solving a generalized eigenvalue problem, $C(t_0)^{-1/2}C(t)C(t_0)^{-1/2}\,\psi^\alpha = \lambda^\alpha(t,t_0)\,\psi^\alpha$, see [5] for details. For sufficiently large times the eigenvalues and -vectors will approach their asymptotic values. The components of a given eigenvector can be interpreted as the coupling strengths of the corresponding operators to the state under consideration. Their magnitude will provide us with information about the magnitude of mixing in the system. We proceed as follows: we first determine the eigenvalues of the 3 by 3 submatrices separately within each of the flavour sectors, where for the moment being we ignore the disconnected contribution in the charmonium sector (see the left hand side of Fig. 4). The light η and its first radial excitation (η') are the lowest two eigenvalues of the submatrix containing only light interpolators and η_c and η_c' within the charmonium sector. We find a diagonalisation of the full 6 by 6 matrix to be numerically unstable and hence restrict ourselves to the basis of the states $(c\bar{c})_{10}$, $(c\bar{c})_{80}$, $(u\bar{u})_5$ and $(u\bar{u})_{40}$ for the full-fledged mixing analysis. In the right hand side of Fig. 4 the effective masses of the lowest three eigenvalues obtained from this basis are shown together with the eigenvalues obtained above, ignoring the mixing effects: within statistical errors no effect is seen. The eigenvectors contain more detailed information about the mixing. We display the components of the ground state η eigenvector on the left hand side of Fig. 5 and those of the η_c eigenvector on the right hand side. Indeed, the η does not contain any statistically significicant admixture from the η_c sector and vice versa.

We conclude that there is no significant η-η_c-mixing and neither are there any other significant flavour singlet effects on the η_c mass. However, the unrealistically heavy pion mass might have affected our conclusion. Runs on $24^3 \times 48$ lattices with $m_\pi \approx 400$ MeV will clarify this issue. Furthermore, mixing with other states like glueballs deserves future attention.

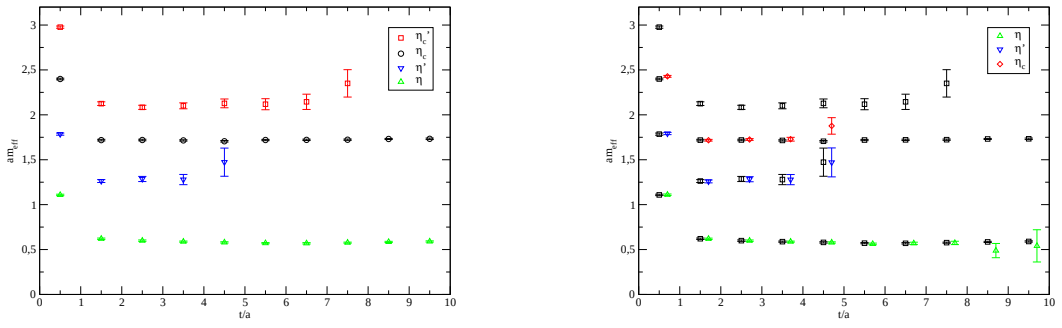

Figure 4: The left plot shows the effective masses of the eigenvalues obtained from diagonalizing the corresponding submatrices. To the right these eigenvalues (in black) are plotted together with the ones obtained from the basis $(c\bar{c})_{10}$, $(c\bar{c})_{80}$, $(u\bar{u})_5$, $(u\bar{u})_{40}$.

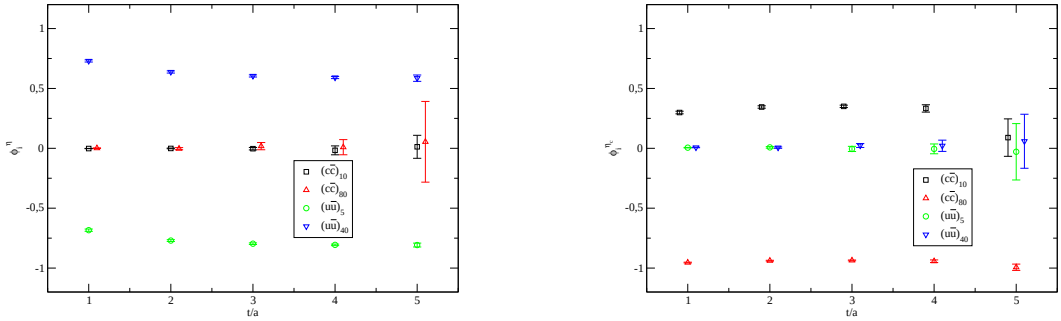

Figure 5: The eigenvector components of the η are displayed on the left, the ones of the η_c on the right.

Acknowledgments

This work was supported by the BMBF (contract 06RY257, GSI-Theory). We thank the DFG Sonderforschungsbereich/Transregio 55 for their support.

References

[1] C. McNeile and C. Michael [UKQCD Collaboration], *Phys. Rev. D* **70** (2004) 034506 [arXiv:hep-lat/0402012].

[2] P. de Forcrand *et al.* [QCD-TARO Collaboration], *JHEP* **0408** (2004) 004 [arXiv:hep-lat/0404016].

[3] L. Levkova and C. DeTar, arXiv:0809.5086 (2008).

[4] S. Gottlieb *et al.*, PoS **LAT2005**, 203 (2006) [arXiv:hep-lat/0510072].

[5] C. Ehmann and G. S. Bali, *PoS* **LAT2007** (2007) 094 [arXiv:0710.0256].

[6] Y. Namekawa *et al.* [PACS-CS Collaboration], *PoS* **LATTICE2008** (2008) 121 [arXiv:0810.2364].

[7] G. S. Bali and P. Boyle, *Phys. Rev. D* **59** (1999) 114504 [arXiv:hep-lat/9809180].

[8] A. Ali Khan *et al.* [QCDSF Collaboration], *Nucl. Phys. B* **689** *(2004) 175* [arXiv:hep-lat/0312030]].

[9] R. G. Edwards and B. Joo [SciDAC Collaboration and LHPC Collaboration and UKQCD Collaboration], *Nucl. Phys. Proc. Suppl.* **140** (2005) 832 [arXiv:hep-lat/0409003].

[10] S. Bernardson, P. McCarty and C. Thron, *Comput. Phys. Commun.* **78** (1993) 256.

[11] J. Foley *et al.*, *Comput. Phys. Commun.* **172** (2005) 145 [arXiv:hep-lat/0505023].

[12] C. Thron, S. J. Dong, K. F. Liu and H. P. Ying, *Phys. Rev. D* **57** (1998) 1642 [hep-lat/9707001].

[13] W. Wilcox, *Nucl. Phys. Proc. Suppl.* **83**, 834 (2000) [arXiv:hep-lat/9908001].

[14] G. S. Bali, H. Neff, T. Düssel, T. Lippert and K. Schilling [SESAM Collaboration], *Phys. Rev. D* **71** (2005) 114513 [arXiv:hep-lat/0505012].

[15] S. Collins, G. S. Bali and A. Schäfer, *PoS* **LAT2007** (2007) 141 [arXiv:0709.3217].